

Available online at www.sciencedirect.com**ScienceDirect**

Procedia Engineering 153 (2016) 180 – 188

**Procedia
Engineering**www.elsevier.com/locate/procedia

XXV Polish – Russian – Slovak Seminar “Theoretical Foundation of Civil Engineering”

On the resistance evaluation of lateral-torsional buckling of bisymmetrical I-section beams using finite element simulations

Marian Giżejowski^a, Radosław Szczerba^a, Marcin Gajewski^a, Zbigniew Stachura^{a*}^a*Warsaw University of Technology, Civil Engineering Department, Al. Armii Ludowej 16, 00-637 Warsaw, Poland*

Abstract

Evaluation of the lateral-torsional buckling resistance of bisymmetrical I-section beams using finite element method was widely discussed in the paper. Numerous FEM simulations with regard to the stability behavior of steel structural elements subjected to bending about the major principal axis were performed. The use of different finite element modeling techniques and their influence on obtained results were presented by the authors. The ultimate state of both perfect and imperfect elements was assessed. Considerations were concerned with hot-rolled wide flange HEB and narrow flange IPE section beams. Idealization of boundary conditions of FEM models complies with the assumptions used in the analytical formulation of stability problems of thin-walled beams. Geometrically and materially nonlinear analyses GMNA and GMNIA preceded by LBA analyses were carried out. Numerical simulations were conducted with use of ABAQUS/ Standard program.

© 2016 The Authors. Published by Elsevier Ltd. This is an open access article under the CC BY-NC-ND license (<http://creativecommons.org/licenses/by-nc-nd/4.0/>).

Peer-review under responsibility of the organizing committee of the XXV Polish – Russian – Slovak Seminar “Theoretical Foundation of Civil Engineering”.

Keywords: LT buckling; steel; FEM modelling; I-section; resistance evaluation

1. Introduction

Evaluation of the ultimate state of both perfect and imperfect beams by the finite element modeling technique requires the discretization of material continuum of the physical object under consideration with finite elements which, depending on the analysis goals, can be of a different type. Modeling includes 1D line elements, 2D planar

* Corresponding author. Tel.: +48-22-825842; fax: +48-22-8256532.
E-mail address: m.gizejowski@il.pw.edu.pl

elements, 3D surface elements and 3D solids of different shapes and with external/internal nodes of different number of degrees of freedom for the calculation of displacement field components and stress resultant components. Usually, the number of finite elements ranges from a few dozen in case of 1D beam elements, thousands to hundreds of millions in case of more sophisticated FEM meshes that include 3D brick elements. The accuracy of modeling depends upon the selection of suitable finite element types and appropriate meshing refinements that convert the geometry of physical object into the set of finite elements with specified number of nodes and node's constraints resulting in a total number of degrees of freedom and in consequence determining the number of differential equations to be solved. In general, the more dense mesh implies the more realistic modeling and more accurate estimation of displacement and stress field components. The biggest challenge in the finite element modeling is the validation and verification processes confirming whether or not the virtual model conforms with the physical object behavior. Validation exercise ensures that there is a close agreement between the behavior of numerical model and the physical object tested, i.e. that there is a sufficient mesh refinement, appropriate finite element types involved and the proper constitutive law selected. Finally, the application of proper numerical methods for solving the set of differential equations linearized in the form of incremental formulation of nonlinear problems is required. In case of analyzed stability problems it allows for tracing the true equilibrium path and checking the stability of equilibrium positions on this path.

Sophisticated finite element simulations are used so widely nowadays as a research tool that it is no longer possible to establish confidence of created numerical models only by application of simplified analytical methods. The verification tests are vital for credibility of finite element simulations, especially in cases where numerical results are more optimistic than the solutions based on conventional engineering knowledge for predicting the results on the safe side.

This paper reports on the stability behavior of steel beams by using numerical simulations and by adopting different levels of accuracy with regard of finite element types and solution procedures of nonlinear stability problem available in the ABAQUS/Standard software. A special attention is paid to slender beams. The differences in the formulation of stability problems using conventional eigenproblem analyses of linear LBA and quadratic QBA of perfect beams, and incremental-iterative nonlinear stability analyses of GMNA of perfect and GMNIA of imperfect beams are presented and the obtained results are widely commented.

2. Assumptions and basic concept of the performed analysis

2.1. Considered member slendernesses, support conditions and load cases, scope of the research

The beams of hot-rolled wide flange HEB 300 and narrow flange IPE 500 sections made of the S235 steel grade are considered. Different element lengths are taken into account that correspond to the minor axis slenderness ratio λ_z from 0.5 to 6.0 for which detailed simulations are performed in order to construct the buckling curves. Simply supported beams subjected to uniform bending about the major principal axis y are considered for the study carried out in this paper. The ultimate state of both perfect and imperfect elements were assessed. Outcomes of numerous FEM simulations were compared with those resulting from application of commonly used analytical formulation of stability problems of thin-walled beams and the Eurocode 3 approach.

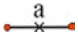
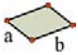
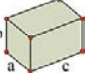
2.2. Material model, geometry discretization by finite elements and modelling of boundary conditions

Material model of the S235 structural steel grade is described with use of an elastic-plastic model with isotropic strain hardening and its uniaxial stress-strain diagram follows that used in [2].

Advanced numerical simulations presented hereafter are based on three modelling techniques, namely applying the thin-walled 3-node beam finite elements which use the quadratic displacement interpolation and allow for the effect of shear strain (FE BM), linear and 4-node thin shell finite elements (FE SM) and 3D linear 8- node brick finite elements (FE 3D). Table 1 presents the list of different finite element types used in numerical simulations, their symbols according to the ABAQUS element library, as well as the number of finite elements and nodes in FEM models in case of longest beams of the HEB 300 cross-section. It is clearly seen that the number of finite elements ranges from a several hundred in case of beam elements to a few millions in case of 3D brick elements.

The geometry discretization by finite elements and modelling of boundary conditions were presented in Fig. 1. Geometric discretization is done in such a way that the convergence of the stability problem to an unknown accurate solution is monotonic and an overall error of the resistance assessment is minimized. For the purposes of comparison, two cases of boundary conditions were considered, namely where the warping of end cross-sections is allowed and where the ends are fully restrained to it. In case of FE BM (Fig. 1a) the warping is allowed through the application of the B32 OS type of finite elements, whereas in case of FE SM (Fig. 1c) the warping is possible due to the use of different modelling tools available in the ABAQUS/Standard software [3]. In case of Figs 1b and 1d the analyzed elements are fully restrained to the warping through the application of the MPC option [3].

Table 1. Finite element types used in numerical calculations.

Type of finite element	Dimensions of finite element	Number of finite elements in FEM model Number of nodes in FEM model		
		$\bar{\lambda}_z = 4.0$	$\bar{\lambda}_z = 5.0$	$\bar{\lambda}_z = 6.0$
B32 OS FE BM	 $a \approx 100 \text{ mm}$	$\frac{291}{583}$	$\frac{363}{727}$	$\frac{436}{873}$
S4R FE SM	 $a \approx b \approx 30 \text{ mm}$	$\frac{29078}{32032}$	$\frac{36330}{37574}$	$\frac{43620}{45107}$
C3D8R FE 3D	 $a \approx b \approx 6.3 \text{ mm},$ $c \approx 11.0 \text{ mm}$	$\frac{1133847}{1567894}$	$\frac{1416987}{1959274}$	$\frac{1700556}{2351247}$

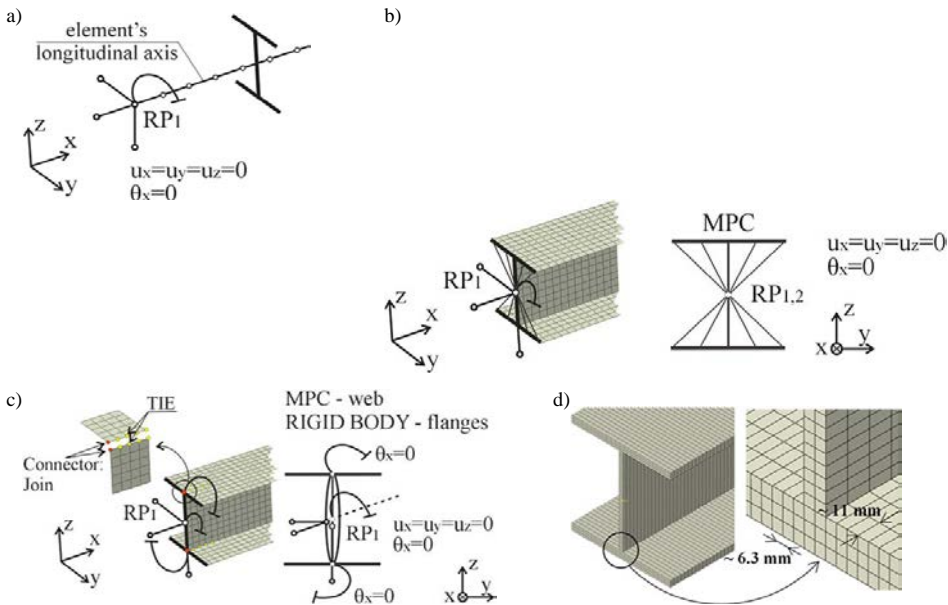


Fig. 1. The geometry discretization and modelling of boundary conditions; a) FE BM; b) FE SM(1); c) FE SM(2); d) FE 3D.

2.3. Nonlinear stability analysis

To solve non-linear boundary value problems of buckling, ABAQUS/Standard program is used, in which the theory of moderately large deformation is implemented and available through an option NLGEOM [3, 4]. The lateral-torsional buckling resistance of considered beams was evaluated based on static overall equilibrium paths. The use of the Newton-Raphson incremental-iterative algorithm with displacement-control allowed to cross the critical point of the load-displacement curves so that the equilibrium paths represent both pre- and post-limit behavior ranges. The rotation of end supports is applied with respect to reference points RP_i incrementally in order to assess the maximum values of bending moment reactions. Therefore, the load-bearing capacity corresponds to the limit point on the path.

In case of perfect elements analyses (GMNA), out-of-plane disturbing factors were firstly applied but of very small value (such that $m_z = M_z / M_{cz,Rk} \approx 0$). This procedure resulted in the assessment of lateral-torsional elastic instability of slender beams subjected to uniform bending about the major principal axis y (see Section 3).

In case of imperfect beams analyses (GMNIA), the imperfection profiles correspond to the first form of elastic lateral-torsional buckling derived from LBA analyses (see Section 4).

The exemplary equilibrium paths with respect to beams of the HEB 300 cross-section, different slenderness ratios $\bar{\lambda}_z$ and various modelling techniques are presented in Fig. 2. Here is the conclusion that the shape of load-deformation curves strongly depends on the slenderness ratio $\bar{\lambda}_z$ of the considered beam.

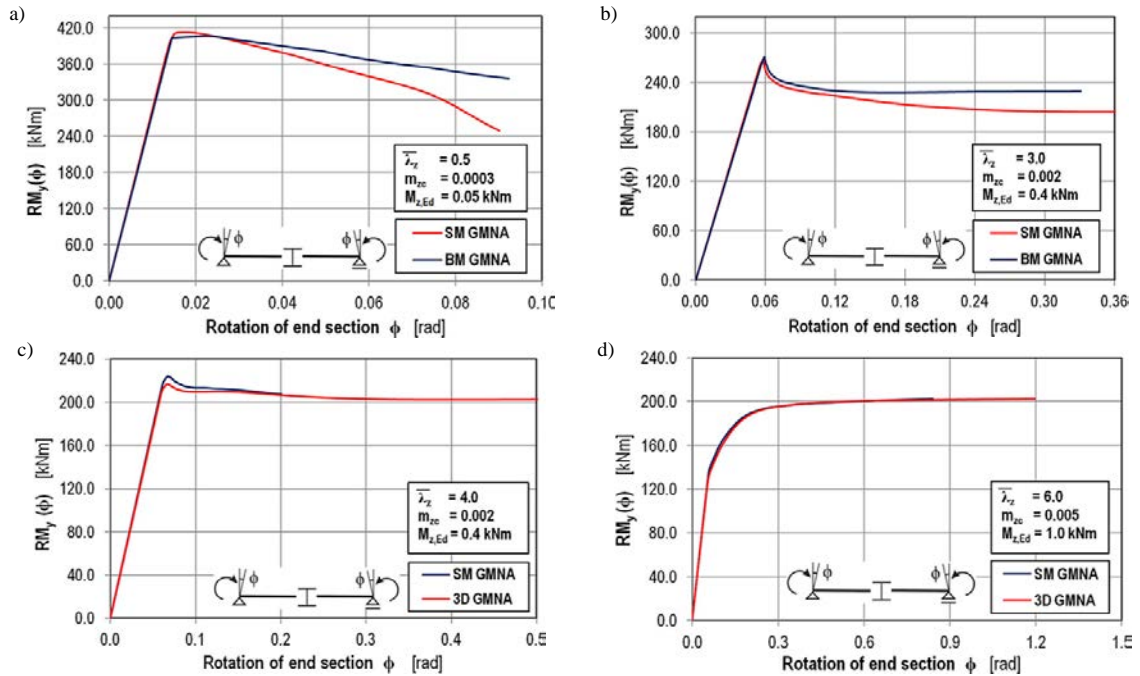


Fig. 2. Load-deformation curves derived from GMNA analyses; a) $\bar{\lambda}_z = 0.5$; b) $\bar{\lambda}_z = 3.0$; c) $\bar{\lambda}_z = 4.0$; d) $\bar{\lambda}_z = 6.0$.

3. Stability problem formulation and analysis of LTB critical state of perfect beams

In the following, the structural behavior of perfect beam elements bent about the major principal axis y is considered. For beams, the ultimate limit state corresponds to lateral-torsional buckling, i.e. $M_{Ed} = M_{b,Rk} / \gamma_{MI}$, where $M_{b,Rk} = \chi_{LT} M_{yc,Rk}$. Thus, the reduction factor χ_{LT} can be expressed as $\chi_{LT} = M_{b,Rk} / M_{yc,Rk}$ and depends upon the slenderness ratio $\bar{\lambda}_{LT}$ according to [5]. On the basis of conventional LBA assumptions, the reduction factor χ_{LT} is calculated as the inversion of the slenderness ratio squared.

A more realistic assessment of the lateral-torsional buckling resistance can be derived from the analytical approximate solution of QBA that results in:

$$\chi_{LT,mod} = \frac{1}{\bar{\lambda}_{LT,mod}^2} = \frac{1}{\sqrt{1 - \frac{I_z}{I_y} \cdot \bar{\lambda}_{LT}^2}} \quad (1)$$

The numerically obtained reduction factors χ_{LT} were evaluated with use of finite element method for selected discrete values of relative slenderness ratios. For this purpose geometrically and materially nonlinear analyses GMNA as well as linear buckling analyses LBA were conducted in the ABAQUS/Standard software. Different finite element modelling techniques were taken into account considering beam, shell and 3D brick element types. The results of numerical calculations are compared with outcomes of conventional LBA and QBA assumptions [equations (1) and (2), respectively], and are presented in Fig. 3a with regard to the HEB 300 cross-section and in Fig. 3b with regard to the IPE 500 cross-section.

In case of results presented in Fig. 3, it is clearly visible that numerical solutions of GMNA analyses tend asymptotically to a non-zero value level of the reduction factor for lateral-torsional buckling, namely $\chi_{LT} \rightarrow W_z / W_y$. This is in contrast to outcomes of LBA and QBA assumptions, in case of which solutions tend asymptotically to zero value ($\chi_{LT} \rightarrow 0$).

In case of the results presented in Fig. 3a for perfect HEB 300 beams ($I_z / I_y = 0.354$, $W_z / W_y = 0.482$), the curves based on $\bar{\lambda}_{LT}$ and $\bar{\lambda}_{LT,mod}$ are distinctly spaced apart from each other.

In case of the results presented in Fig. 3b for perfect IPE 500 beams, due to the high slenderness of the cross-section ($I_z / I_y = 0.046$, $W_z / W_y = 0.158$), all results are close to each other.

One may also notice that warping deformations at beam ends are of secondary importance in case of very long elements (results in case of $\bar{\lambda}_z = 4.0, 5.0, 6.0$ in Fig. 3a).

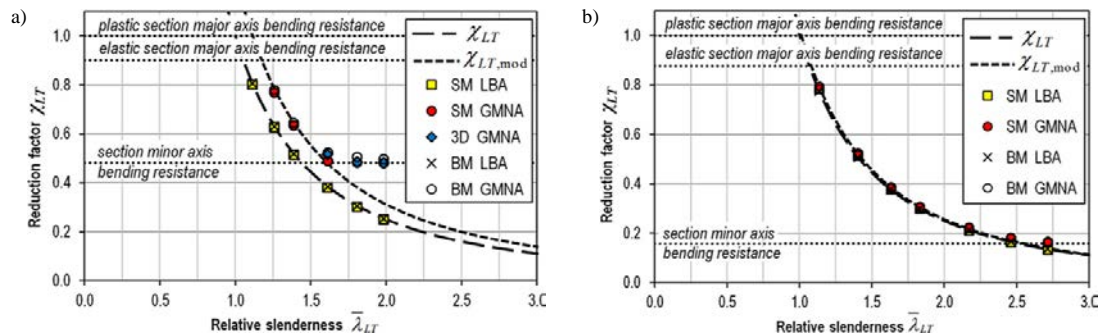


Fig. 3. Reduction factor χ_{LT} as a function of $\bar{\lambda}_{LT}$ in case of GMNA analyses; a) HEB 300; b) IPE 500.

4. Stability problem formulation and analysis of LTB resistance of imperfect beams

4.1. Modelling of profile imperfection

The profile of imperfections for the beam imperfect structural model is that of directly implied in Eurocode 3, Part 1-1 [5]. It is derived from the model of imperfect beams under uniform bending that leads to the following magnitude of the minor axis bending amplitude (see [6,7]):

$$e_{0,LT} = \frac{\alpha_{LT} (\bar{\lambda}_{LT} - 0,2)}{\frac{M_{cy,Rk}}{B_{c,Rk}} \left[1 + \frac{N_{cr,z}}{M_{cr}} \left(\frac{B_{c,Rk}}{M_{cz,Rk}} - \frac{GI_T}{M_{cr}} \right) \right]}, \tag{2}$$

$N_{cr,z}$, $N_{cr,T}$ = elastic critical forces for the relevant buckling modes; $B_{c,Rk}$ = bimoment section resistance; $M_{cy,Rk}$, $M_{cz,Rk}$ = moment section resistances about y-y and z-z axes, respectively; α_{LT} = imperfection parameter in relation to the section geometry and fabrication process (other symbols according to Eurocode 3, Part 1-1 [5]).

In case of numerical calculations, the geometry of an imperfect element in the initial configuration was adopted as the scaled first buckling mode derived from LBA analysis (in case of uniform bending), as shown in Fig. 4.

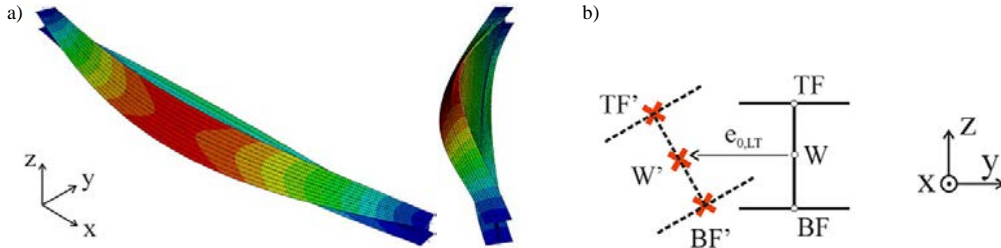


Fig. 4. a) the first buckling mode corresponding to lateral-torsional buckling; b) the imperfection amplitude $e_{0,LT}$.

4.2. The lateral-torsional buckling curves

In the following, results obtained for the resistance of imperfect structural elements under the uniform bending moment $M_{y,Ed}$ are presented. The outcomes are given for beams of both HEB 300 and IPE 500 cross-sections. The imperfection profiles correspond to the first form of elastic lateral-torsional buckling derived from LBA analysis, as described above.

Table 2 presents the comparison of GMNA and GMNIA analyses results in case of shell modelling technique. Obtained lateral-torsional buckling resistances as well as values of initial imperfection amplitudes were given. In turn, the influence of initial imperfection on the post-buckling deformation state in case of the HEB 300 cross-section beam and $\bar{\lambda}_z = 1$ is shown in Fig. 5.

Table 2. Comparison of GMNA and GMNIA analyses results in case of shell modelling technique.

Shell modelling technique FE SM		Relative slenderness $\bar{\lambda}_z$							
		1.0	1.5	2.0	2.5	3.0	4.0	5.0	6.0
HEB 300 curve "a"	$e_{0,LT}$ [mm]	7.9	16.5	27.7	41.2	56.7	93.1	135.9	184.2
	GMNA [kNm]	<u>417.5</u>	<u>412.8</u>	<u>412.3</u>	<u>321.2</u>	<u>266.8</u>	<u>205.3</u>	<u>203.4</u>	<u>202.5</u>
	GMNIA [kNm]	365.2	317.3	273.6	240.0	218.4	203.6	206.3	205.5
IPE 500 curve "b"	$e_{0,LT}$ [mm]	5.0	9.3	14.9	21.7	29.6	48.6	71.4	97.6
	GMNA [kNm]	<u>485.0</u>	<u>393.7</u>	<u>259.9</u>	<u>191.7</u>	<u>152.9</u>	<u>110.6</u>	<u>90.7</u>	<u>80.7</u>
	GMNIA [kNm]	349.6	251.4	188.6	150.5	126.8	98.8	85.6	78.5

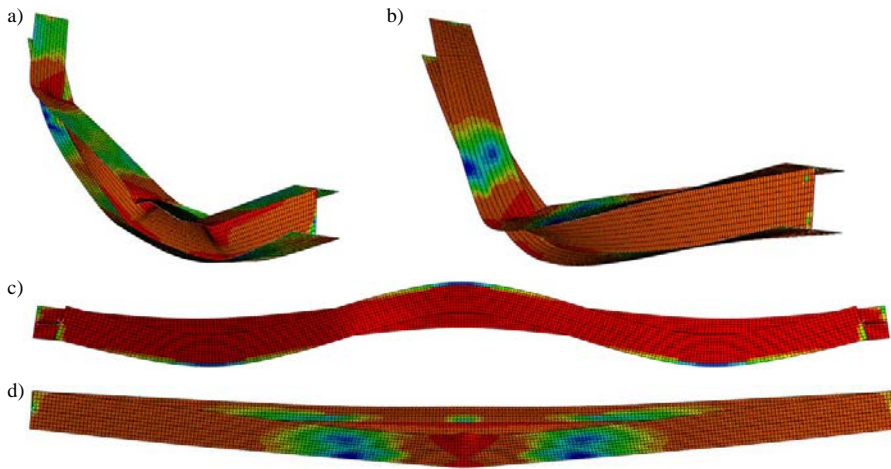


Fig. 5. Post-buckling deformation in case of the HEB 300 cross-section and $\bar{\lambda}_z = 1.0$; a); c) GMNA analysis; b); d) GMNIA analysis; deformation state scale factor = 1.0.

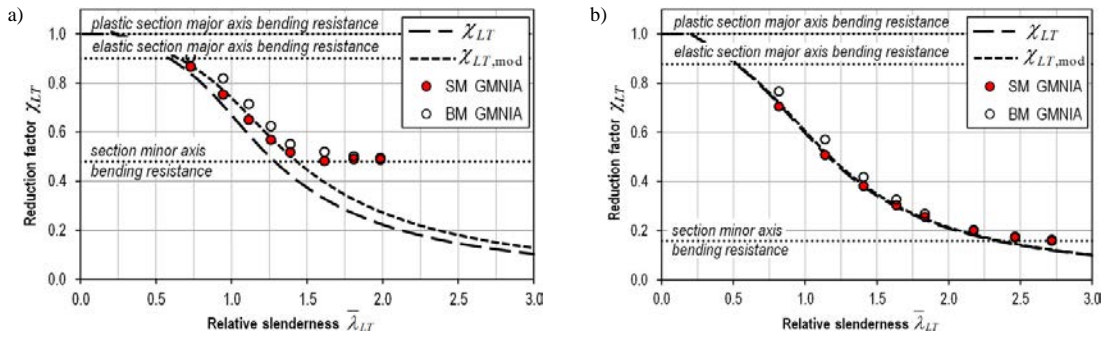
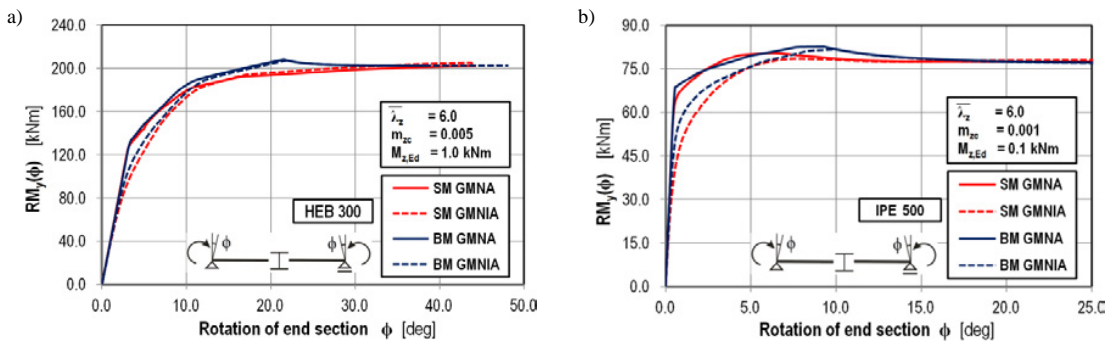


Fig. 6. Reduction factor χ_{LT} as a function of $\bar{\lambda}_{LT}$ in case of GMNIA analyses; a) HEB 300; b) IPE 500.



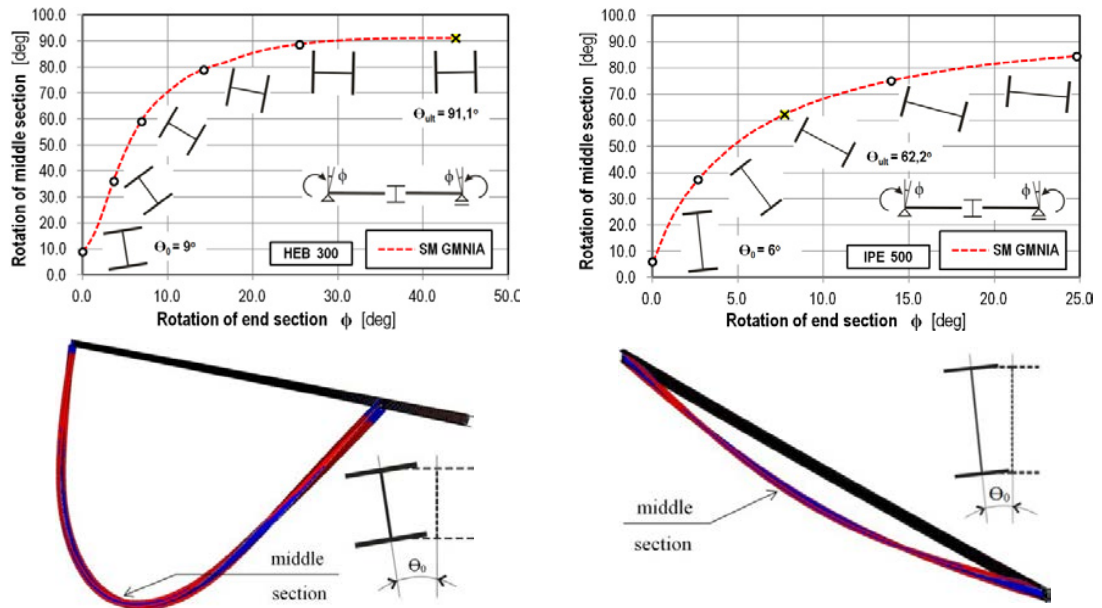


Fig. 7. Results of GMNIA analyses in case of $\bar{\lambda}_z = 6.0$; a) HEB 300; b) IPE 500; Θ_0 - initial imperfection, deformation state scale factor = 1.0.

The verification of obtained results is presented in Fig. 6a for the HEB 300 cross-section and in Fig. 6b for the IPE 500 cross-section in such a way that numerical results for $M_{z,Ed} = 0$ are compared with the respective Eurocode's buckling curves ("a" and "b", respectively). Conclusions are similar to those from the GMNA simulations. In case of the results presented in Figure 6a for imperfect HEB 300 beams ($I_z / I_y = 0.354$), the Eurocode's curves "a" based on $\bar{\lambda}_{LT}$ and $\bar{\lambda}_{LT,mod}$ are distinctively different, whereas in case of imperfect IPE 500 beams ($I_z / I_y = 0.046$), the obtained results are close to each other (the Eurocode's curves "b" are practically overlapping). In case of the HEB 300 cross-section, the results from FEM simulations are close to the Eurocode's buckling curve based on the slenderness $\bar{\lambda}_{LT,mod}$ and they are distinctively away from that based on the slenderness $\bar{\lambda}_{LT}$. Furthermore, the beam resistances obtained numerically from BM based simulations are placed above those of SM based.

Regarding the results presented in Figs. 3 and 6 and also in Tab. 2, one may notice that the influence of imperfections on lateral-torsional buckling resistance is significant only in case of semi-slender elements and is negligible for very long beams. Furthermore, it is shown in Fig. 7 that the introduction of initial imperfection profile caused the plastic hinge formation only at the middle beam's section, whereas in case of perfect element there are three plastic hinges clearly visible in Fig. 5.

Figure 7 explains why the numerical solutions of GMNA and GMNIA analyses tend asymptotically to a non-zero level of the reduction factor for lateral-torsional buckling, namely $\chi_{LT} \rightarrow W_z / W_y$. The present simulations proved that the HEB 300 section of long-span beams may practically rotate at the ultimate limit state of about 90° while the IPE 500 rotates about 60° about the longitudinal x -axis. This is the explanation why the buckling strength reduction factor for wide flange I-section slender beams tends to asymptotically approach the higher value than that for narrow flange I-section beams. The wide flange I-section imperfect beams are subjected to larger in-plane displacements prior to the LTB state than those of narrow flange I-section imperfect beams. Therefore, the large in-plane displacements of former beams are associated with larger twist rotations prior to the limit point on the beam's equilibrium path. Contrarily, the latter beams are subjected to smaller twist rotations at the ultimate limit state.

5. Concluding remarks

Elastic and elastic-plastic overall instability problems of steel I-section beams subjected to bending about major principal axis with regard to both perfect and imperfect elements are dealt with in this paper. The authors indicated and discussed several aspects that influence the numerical assessment of lateral-torsional buckling resistance of steel I-section beams.

Observations and conclusions presented in the paper may be useful for the revision of the Eurocode's approach that is based on the conventional linear buckling theory. Due to this fact, results obtained for wide flange section beams are underestimated. The proposal for a new method of the lateral-torsional buckling resistance evaluation of steel I-section beams is presented by the authors in [8]. Postulated method is based on the nonlinear buckling theory and is valid for the design verification of both stocky and slender imperfect beams. Study presented in the paper can be extended to the case of two directional bending and beam resistance interaction curves, as described in [9].

References

- [1] Simoes da Silva L., Simoes R., Gervasio H., Design of steel structures, Eurocode 3: Design of steel structures, Part 1-1: General rules and rules for buildings. ECCS Eurocode Design Manual, Ernst & Sohn, 2010.
- [2] Giżejowski M.A., Szczerba R., Gajewski M., Stachura Z., Beam-column resistance interaction criteria for in-plane bending and compression, *Procedia Engineering*, Special Issue (eds. Jemiolo S., Gajewski, M. & Krzeminski, M.), *Open Access Journal*, Elsevier, 2015, Vol. 111, pp. 254-261.
- [3] ABAQUS/Standard *User's manual*, Version 6.1., Hibbit, Karlsson and Sorensen, Inc., Pawtucket, 2000.
- [4] ABAQUS *Theory manual*, Version 6.1., Hibbit, Karlsson and Sorensen, Inc., Pawtucket, 2000.
- [5] EN 1993-1-1, Eurocode 3: Design of Steel Structures, Part 1-1: General rules and rules for buildings. Brussels: European Committee for Standardization, 2005.
- [6] Trahair N.S., *Flexural-torsional buckling of structures*, Boca Raton: CRC Press, 1993.
- [7] Rykaluk K., *Stability problems of metal structures*, Wrocław, Dolnośląskie Wydawnictwo Edukacyjne, 2012 [in Polish].
- [8] Giżejowski M.A., Gajewski M., Stachura Z., Szczerba R., On the evaluation of lateral-torsional buckling of steel I-section beams, *Inżynieria i Budownictwo* [submitted, in Polish].
- [9] Giżejowski M.A., Szczerba R., Gajewski M., Stachura Z., Numerical study of buckling resistance of steel I-section members under two directional bending, in: *Proceedings of the 6th International Conference on Structural Engineering, Mechanics and Computation (SEMC)*, 2016 [in press].